Personal Account

DOI: 10.1002/tcr.201800008

THE CHEMICAL RECORD

Carbon Nanomaterials in Direct Liquid Fuel Cells

Huayun Du,[a] Cindy Xinxin Zhao,[b] Jing Lin,*[c] Jiang Guo,*[d] Bin Wang,[d] Zhen Hu,*[e] Qian Shao,[f] Duo Pan,[f] Evan K. Wujcik,[g] and Zhanhu Guo*[b]

Abstract: Fuel cells have attracted more attentions due to many advantages they can provide, including high energy efficiency and low environmental burden. To form a stable, low cost and efficient catalyst, we presented here the state of the art of electrocatalyst fabrication approaches, involving carbon nanotubes and their multifunctional nanocomposites incorporated with noble metals, such as Pt, Pd, Au, their binary and ternary systems. Both fuel oxidation reactions and oxygen reduction reactions were emphasized with comprehensive examples and future prospects.

Keywords: Fuel cells, catalysts, fuel oxidation, oxygen reduction

[a] *H. Du*
College of Materials Science and Engineering, Taiyuan University of Technology, Taiyuan 030024, China
[b] *C. X. Zhao, Z. Guo*
Integrated Composites Laboratory (ICL), Department of Chemical & Biomolecular Engineering, University of Tennessee, Knoxville, TN 37976, USA
E-mail: zguo10@utk.edu
[c] *J. Lin*
School of Chemistry and Chemical Engineering, Guangzhou University, Guangzhou 510006, P.R. China
E-mail: linjing@gzhu.edu.cn
[d] *J. Guo, B. Wang*
Engineered Multifunctional Composites (EMC) Nanotech. LLC, Knoxville, TN 37934 USA
E-mail: jeremyjiangguo@gmail.com
[e] *Z. Hu*
School of Chemistry and Chemical Engineering, MIIT Key Laboratory of Critical Materials Technology for New Energy Conversion and Storage, Harbin Institute of Technology, Harbin 150001, China
E-mail: huzhen@hit.edu.cn
[f] *Q. Shao, D. Pan*
College of Chemical and Environmental Engineering, Shandong University of Science and Technology, Qingdao 266590, China
[g] *E. K. Wujcik*
Materials Engineering and Nanosensor [MEAN] Laboratory, Department of Chemical and Biological Engineering, University of Alabama, Tuscaloosa, AL, USA

1. Introduction

The ever-increasing worldwide use of fossil fuels is one of the most profitable yet injurious phenomena in modern society. The combustion of hydrocarbons, such as coal, oil and natural gas, upon which the world depends mostly for our energy demands, was adopted centuries before its capacity and environmental costs had been recognized. These reserves are limited in supply and greenhouse gases are released by burning fossil fuels, causing poor air quality of many urban areas, and intensifying the threat of global warming. Therefore, a major strategic shift towards renewable energy sources is necessary, to achieve more advances and positively impact the future energy applications, including solar cells[1–5] and electrochemical energy storage systems, for example, electrochemical capacitors,[6,7] batteries[8] and our focus- fuel cells.[9]

As a promising energy conversion technology for the next century, the basic design of a typical fuel cell involves an anode, to which the fuel is supplied; a cathode filled with an oxidant, typically oxygen; and an electrolyte, which only allows the flow of ions between the anode and cathode. The net chemical reaction is exactly the same as if the fuel is burned, but the flow of electrons is produced by spatially separating the reactants. Unlike combustion engines, the efficiency of fuel cells is not restricted by the Carnot efficiency limit. Instead, the efficiency of fuel cells is determined by the ratio of the Gibbs function change to the enthalpy change in the overall cell reaction. For a hydrogen/

oxygen fuel cell operating at the standard conditions, the cell efficiency can be calculated according to Equation:

$$\eta = \frac{\Delta G^0}{\Delta H^0} = \frac{237.1\ kJ/mole}{285.8\ kJ/mole} = 0.83$$

This value is obviously higher than that normally obtained on an internal combustion engine. In practical operations, fuel cell efficiencies can be more conveniently measured by using the voltage efficiency, the ratio of the actual voltage under operating conditions to the theoretical cell voltage:

$$\eta = V/1.23$$

There are different types of fuel cells which are distinguished by their fuels, electrolytes, different ions to transport charges from one electrode to the other. Most fuel cells consume hydrogen or hydrogen-rich forms, sufficient reactive fuels including methane,[10] methanol,[11,12] and ethanol,[13,14] and biomass such as glucose[15,16] and cellulose.[17] Among all major types of fuel cells, proton-exchange membrane fuel cells, phosphoric acid fuel cells and solid oxide ceramic fuel cells have already been commercially available in residential and industrial settings, such as portable power generation, stationary power generation, and power for transportation. However, their drawbacks still exist, typically including the CO poisoning, water management, and noble catalyst. Great efforts are being done these days to develop highly efficient electrocatalysts of easy accessibility, CO tolerance and low cost.

On the other hand, carbon nanostructures and their derivatives, such as fullerenes,[18,19] carbon nanotubes,[20,21] and graphene,[22,23] have been widely studied since 1980s. Their large aspect ratio, high specific surface area, and tunable electrical conductivity from semiconductor to metal-like, make these carbon nanomaterials good candidates in the research of light emitting devices,[24] solar cells,[2] sensing devices,[25] supercapacitors,[6] and fuel cells.[7] Although their size is very small, the quantum effects are important and the incorporation of pristine and functionalized carbon nanostructures to different materials can sometimes double the electrical and thermal properties for a load of only 1 %. These properties are strongly depending on the atomic arrangement, size, morphology and distribution. Each group of carbon nanomaterials has its own distinct features. For instance, the observation of highly increased photoconductivities upon C_{60} addition to conjugated polymers, led to the development of polymer-fullerene heterojunction. However, the domain size of C_{60} needs to be well-controlled for the optimal bicontinuous network of donor and acceptor phases.[2,3,26–31] Despite of the tubular porous structure and superior electrical property approaching that of copper, the applications of CNTs in the electrochemical capacitors are still limited by the high production costs. The 2D graphene sheets, the Nobel Prize winner topic of 2010, are reported as the strongest material ever tested; however, they are thermodynamically unstable and easy to get restacked.

Owing to further understanding towards quantum physics and chemistry, we are now able to manipulate these carbon nanomaterials, by controlled synthesis, functionalization, and self-assembly techniques. Here, the state of the art of an electrocatalyst fabrication approach will be presented; carbon nanotubes and their multifunctional composites are incorporated with noble metals, to form a stable and efficient catalyst used in direct liquid fuel cells.

2. Fundamentals of Fuel Cells

Fuel cells all share a common theme: electrochemical oxidation of a fuel. Figure 1 shows a typical proton exchange member fuel cell (PEMFC), where hydrogen and oxygen move to the electrolyte though the electrodes. Electrons are produced at the anode/electrolyte interface, pass through an external circuit and then are consumed at the cathode/electrolyte interface. The reduction of hydrogen gives birth to two protons, which are free to migrate through the electrolyte towards the cathode, where oxygen molecules are dissociated into atoms, and combine with both electrons and the migrating protons to form water.

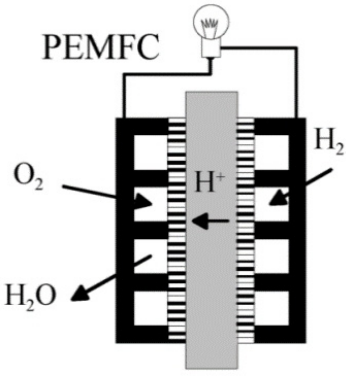

Figure 1. A typical PEMFC consumes reactants and generates a current.

The performance of a fuel cell is evaluated by a polarization curve, where the DC voltage delivered at the electrodes as a function of the current density is drawn by the external load. One measure of the energy conversion efficiency is the ratio of the actual voltage at a given current density to the maximum voltage obtained under an open circuit condition. According to the thermodynamics and

electrochemisty, PEMFC can be written by two half reactions,

Oxidation half reaction : $2H_2 \rightarrow 4H^+ + 4e^-$

Reduction half reaction : $O_2 + 4H^+ + 4e^- \rightarrow 2H_2O$

Overall cell reaction : $2H_2 + O_2 \rightarrow 2H_2O$

And the energy formation for the overall reaction is $-\Delta H^o = 286$ kJ/mol and $-\Delta G^o = 237$ kJ/mol. Therefore, the maximum open circuit voltage at an ideal condition can be calculated as $E = \Delta G^o/nF$, where n is the number of electrons transferred in the reaction, and F the Faraday constant. Therefore, the theoretical open circuit voltage (V_{oc}) would be 1.23 V. The maximum efficiency occurs under V_{oc} conditions, which is theoretically 83 . However, in reality fuel cells achieve their highest output voltage at V_{oc} conditions and the voltage drops off with increasing the current density, as shown by Figure 2. The losses are mainly classified as activation, ohmic and concentration overpotentials. Activation overpotential is caused by the slowness of the reaction taking place on the electrode surface; and ohmic overpotential accompanies the passage of current through various components of the fuel cell and is due to the electrical resistance; whereas concentration overpotential is developed when the electrode reactions become limited by the availability of reactants at the active electrode/electrolyte interface.

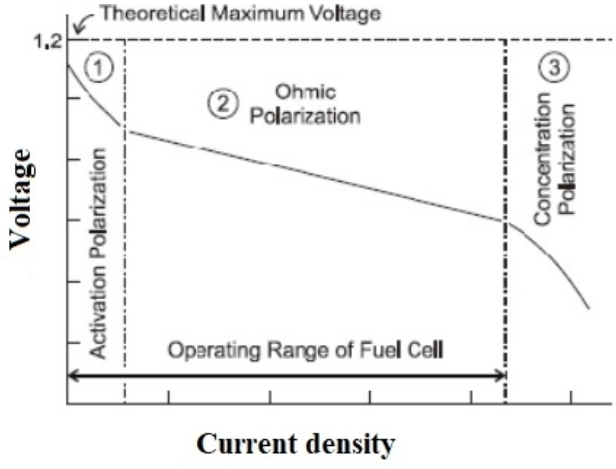

Figure 2. The polarization curve shows the electrochemical efficiency of the fuel cell at any operating current and three overpotentials.

Ever since the first application of Nafion in fuel cells and the successful deposition of Pt catalyst onto the membrane in the 1960s, a lot of research has gone into improving the performance an reducing Pt catalyst loading. The first PEMFCs utilized Pt/carbon black, with particle size of 50–100 nm and physical surface area of 10 m^2g^{-1}, requiring a loading of 4 $mg_{Pt}cm^{-2}$. Subsequently, carbon supported electrocatalysts were introduced, which consisted of smaller metal nanoparticles (< 10 nm) dispersed on high surface area support materials, allowing excellent dispersion of Pt nanoparticles and decreasing the loadings. At present, the lowest Pt catalyst loading achieved without compromising the performance is 0.15 $mg_{Pt}cm^{-2}$. Meanwhile, it is found that Pt and Pt group metals have intermediate values of hydrogen absorption enthalpy, and therefore shows the highest catalytic activity among the transition metals. Our group has been working on the catalysts and their supporting materials, to improve the fuel cell performance, lower the cost and enhance the durability.

3. Carbon Nanomaterials in Direct Liquid Fuel Cells

Nowadays many attentions have been paid to direct liquid fuel cells, due to their advantages of high energy conversion efficiency, low operating temperature and low environment pollution. They also have the subcategory, according to the fuels applied to the anode, i.e., direct methanol fuel cells, direct ethanol fuel cells and direct formic acid fuel cells, etc.

For methanol oxidation reaction, Pt is the best catalyst although it is known for the disadvantages of high cost and CO poisoning effect. To make full use of Pt, size controlled nanostructures with certain distribution patterns are desired to enlarge the effective surface area. The control of particle size and distributions, however, is hard due to the aggregation nature of nanoparticles. Therefore, surfactants or polymer holders are introduced to form an even distribution of nanoparticles, which inevitably increases the internal resistance of the fuel cells by blocking the electrolyte contact. To overcome the above difficulties, Pt decorated CNTs were prepared by an atomic layer deposition method.[11] An increased D-band/G band ratio by Raman spectra suggested that the interaction between Pt and CNT was increased with increasing the deposition circle. Ultrafine Pt nanoparticle size was confirmed by the absence of Pt peaks in the XRD patterns before and after thermal annealing. A further increase of annealing temperature introduced the agglomeration of Pt nanoparticles as shown by TEM, thus reducing the catalytic activity towards methanol oxidation. It is found that the optimal Pt/CNT catalyst was obtained at 100 deposition circles and 100 °C annealing condition, with the highest peak current density of 2000 mA/mg_{Pt}.

We also introduced Pd nanoparticles stabilized by MWNT–COOH without surfactant.[12] The increased D-band/G band ratio as well as the decreased oxygen containing species ratio suggested the interaction between Pd nano-

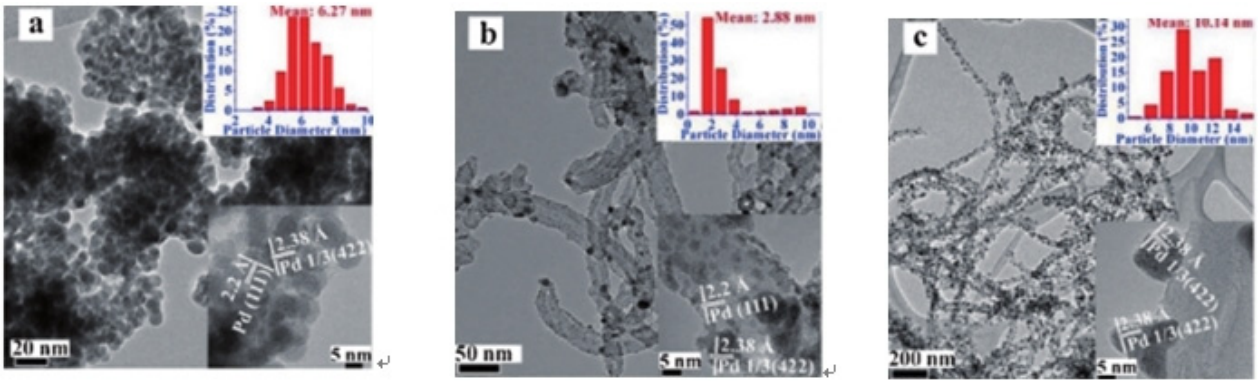

Figure 3. TEM microstructures of a) bare Pd NPs, b) Pd–MWNTs, and c) Pd–MWNT–COOH. Inset: particle-size histograms (top) and HRTEM images (bottom) of the corresponding nanocatalysts. The HRTEM images provide a closer view of the lattice fringes of the Pd NPs. Reprint with permission from Ref. [12].

particles and COOH groups. The MWNT–COOH behaved as an anchor to secure the dispersion of Pd nanoparticles shown by TEM, Figure 3. The effects of methanol, KOH concentration and temperature on the Pd/MWNT–COOH for the methanol oxidation were evaluated and an optimum peak current density was determined by means of a balanced adsorption of methanol and hydroxide on the electrode surface. The catalyst performance can be improved by increasing the temperature due to enhanced reaction kinetics.

Ethanol is an excellent alternative to methanol due to its nontoxicity, easy production from agricultural products, high energy density, and low fuel crossover that is often encountered in the methanol-based fuel cells. Recently, the catalytic activity of Pd towards ethanol oxidation reaction in alkaline media was found to be higher than that of Pt, leading to the developments of Pd or Pd based alloy or composite nanocatalysts.

We first worked on the Pt–Pd bimetallic nanoparticles supported by MWCNTs.[32] The obtained catalysts with various feed molar ratios were characterized by X-ray diffraction, scanning electron microscopy and TEM, showing an average particle size of ~4.0 nm dispersed uniformly on the MWCNT surface. In 1.0 M KOH solution, the onset potential for ethanol oxidation using Pt_3Pd_3/MWCNTs was found to be approximately 200 mV lower and the peak current 10 times higher than those obtained using Pt/MWCNTs catalyst, owing largely to the existence of PdO in the Pt_3Pd_3/MWCNTs.

Utilizing similar techniques but room temperature ionic liquid as the solvent, Pd–Ni nanocomposites on MWCNTs were synthesized using ionic liquid as the solvent, with an average crystal size of ~7.0 nm uniformly distributed on the top of MWCNTs.[33] It was also revealed that the onset potential for ethanol oxidation using $Pd_1Ni_{1.5}$/MWCNTs was about 80 mV lower and the peak current 3 times higher when compared with those of Pd/MWCNTs. From the point of electrochemistry, Ni is prone to release electrons to form Ni^{2+}, and in alkaline solution $Ni(OH)_2$ may form close to these $Pd_1Ni_{1.5}$ particles, and generate NiOOH in a higher potential. A mini cell may form where Ni serves as the negative electrode and Pd as the positive one, creating a micro-environment for the interface of $Pd_1Ni_{1.5}$/MWCNT, which provides a possible explanation for many binary or ternary composite catalyst systems.

In 2014, we continued to study the binary catalyst systems, and synthesized the bimetallic $PtNi_x$ nanocomposites via a hydrothermal reaction, where MWCNTs served as reductants.[34] $PtNi_x$ nanoparticles of 6–13 nm were found to be immobilized on the MWCNTs, showing an onset potential for ethanol oxidation of 190 mV lower and the peak current 2.5 times higher than those of Pt/MWCNTs.

Inspired by these interesting findings, a catalyst denoted as PdO/MWCNTs was prepared, by dry-grinding the mixture of PdO and MWCNTs, which showed the smallest particle sizes among all samples (Figure 4), and ultrahigh electrocatalytic activity towards EOR.[14] The forward peak current density reached 5029 $mA\,mg^{-1}$ at a scan rate of 50 $mV\,s^{-1}$ in 1.0 M KOH, which was approximately 2.1 times higher than the reported value obtained on commercial Pt/C catalysts. The easier hydrogen evolution process on PdO/MWCNTs was regarded as the reason for its excellent catalytic performance. The preliminary work also suggested the as-prepared PdO/MWCNTs have the catalytic activity towards both methanol and formic acid oxidation reactions.

Later on, we synthesized the Pd nanoparticle decorated MWNTs–COOH by thermally decomposing palladium acetylacetonate in a refluxing xylene solution with dispersed MWNTs–COOH.[13] By Raman spectroscopy, an increased ratio of D band/G band, as well as a decreased ratio of oxygen containing functional groups (COOH, C–O and C=

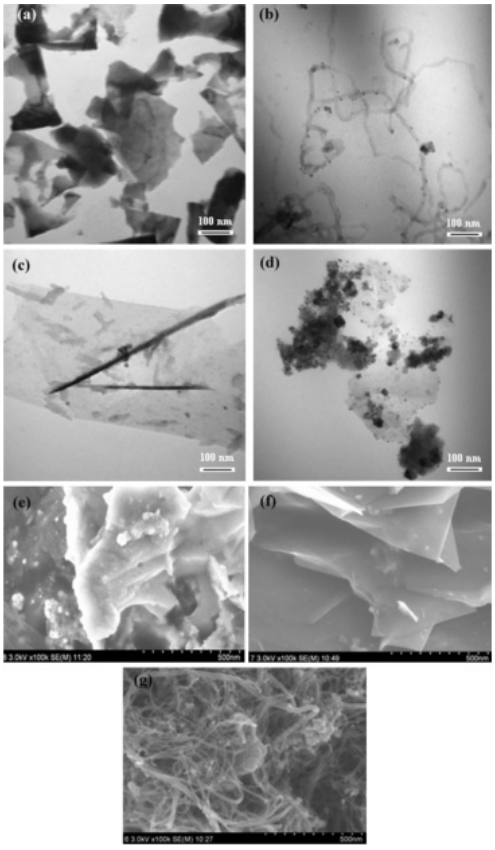

Figure 4. TEM images for a) as-received PdO, b) PdO/MWCNTs, c) PdO/graphene, and d) PdO/graphite. SEM images for e) catalyst PdO/graphite, f) PdO/graphene, and g) PdO/MWCNTs. Reprint with permission from Ref. [14].

O) were discovered, suggesting that the defects on MWNTs were increased during fabrication. Various distributions of Pd NPs on the MWNTs and a trend of the increased Pd particle size with increasing the Pd loading were observed by TEM, leading to an optimal $Pd(acac)_2$ to Pd conversion of 76.21%, when the initial precursor ratio of $Pd(acac)_2$ to MWNTs was 2:1. The Pd/MWNTs-2:1 catalysts showed the highest Pd mass-based peak current density of 1.23 A/mg_{Pd} and stable current density of 0.175 A/mg_{Pd}. The impedance spectroscopy and Tafel characterization results further confirmed the reduced charge-transfer resistance and increased reaction kinetics with increasing the Pd loading.

The latest progress on ethanol oxidation reaction was made in late 2015, when we deposited ultrafine FePd nanoalloys on γ-Fe_2O_3, and further anchored the FePd–Fe_2O_3 on MWNTs–COOH by one-pot solution based method as in situ thermally decomposing $Pd(acac)_2$ and $Fe(CO)_5$ in a refluxing dimethylformamide solution in the presence of MWNTs–COOH, as described in Figure 5.[35] Compared with Pd/MWNTs, the peak current density showed a 3.65 fold increase. The downward shifted D-band center of FePd alloy, easily formed oxygen containing species on Fe_2O_3, and the stabilizing ability of MWNTs, contributed to the enhanced poisoning tolerance and reduced charge transfer resistance.

Unlike direct methanol/ethanol fuel cells, direct formic acid fuel cells can operate in acidic solutions. Formic acid oxidation reaction primarily depends on the electrodes, electrolytes and operating conditions. We employed the Pd decorated MWCNTs to explore the effects of operation conditions on the reaction, such as formic acid and sulfuric acid concentration, and temperature.[36] The enhanced electrocatalytic activity of Pd/MWNTs was attributed to the hydrogen adsorption in the low potential and oxidation of poisoning species in high potential during cyclic voltammetry. The balance of HCOOH and H_2SO_4 absorption was achieved, in order to obtain the best electrode performance. Another attempt was the bimetallic PdNi nanoparticles decorated MWCNTs.[37] Different compositions of the catalyst were synthesized by thermal decomposition using room temperature ionic liquids as the solvent. The microscopic images revealed that the nanoparticles were evenly distributed on the nanotube surface, with an average particle size of 8.0 nm. The peak current on the Pd_3Ni_2/MWCNTs in 0.5 M H_2SO_4 was approximately 4 times that of the Pd/MWCNTs, due to the lower electrode potential and easier hydrogen evolution.

Besides Pt and Pd, Au has also been intensively studied in order to reduce the production cost in the anode, for fuel oxidation, and in the cathode, for oxygen reduction. For the first time, Au composite particles embedded with MWCNTs were fabricated with an average diameter of about 500 nm by a one-step hydrothermal process of $AuCl_3$ in a MWCNT aqueous solution.[38] Some MWCNTs inserted into the Au composite, as reflected in Figure 6. The shape of CVs for ethanol oxidation differs from the literature, showing the catalytic capability of Au/MWCNTs toward ethanol oxidation reaction in alkaline solution. Moreover, the highly crystalline Au composites prepared by the pyrolysis of $AuCl_3$ dissolved in room temperature ionic liquid in the presence of MWCNTs can electrocatalyze the oxygen reduction reaction in neutral solution, and the catalytic activity was found to be closely related to the pyrolysis time.[39]

4. Conclusion and Perspectives

We provided here the state of the art of electrocatalyst fabrication approaches used for direct liquid fuel cells, involving carbon nanotubes and their multifunctional composites. The combinations of noble metal nanoparticles and carbon nanotubes can hopefully expand the promising applications of fuel cells in portable power generation and

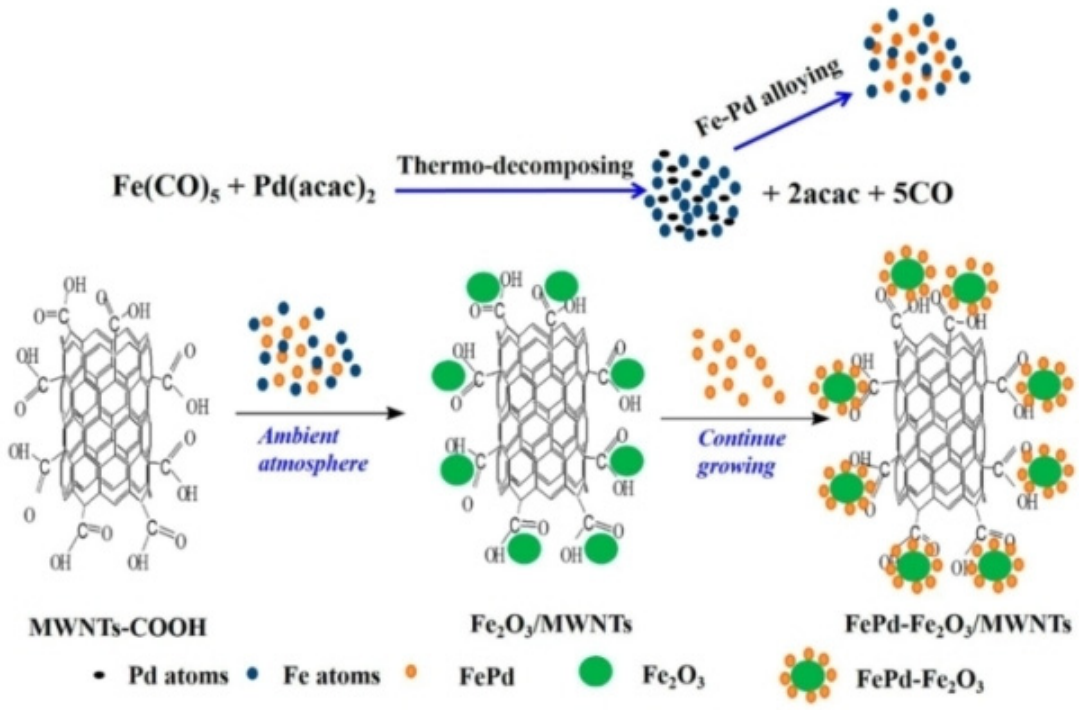

Figure 5. Schematic representation for the synthesis of FePd–Fe_2O_3/MWNTs nanocatalysts. Reprint with permission from Ref. [35].

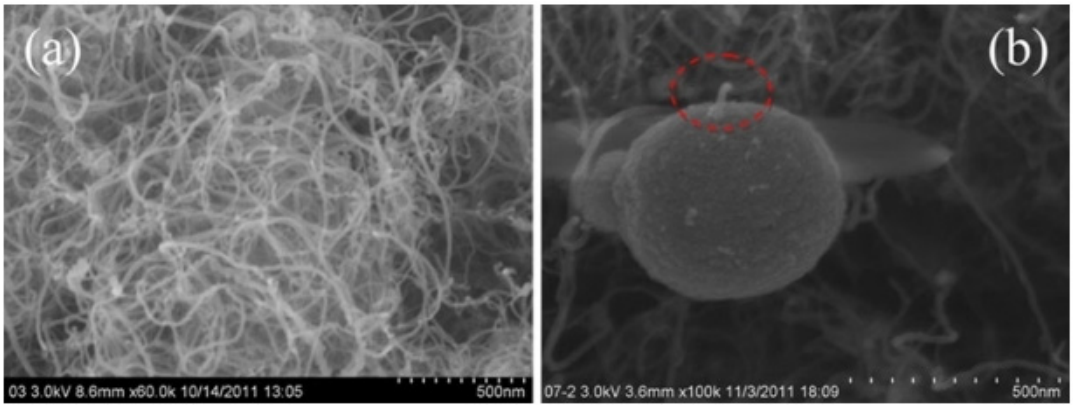

Figure 6. SEM images for (a) pure MWCNTs and (b) the obtained MWCNTs-inserted Au composite particles prepared by hydrothermal process for 2 h. Reprint with permission from Ref. [38].

portable electronics. Meanwhile, carbon-based nanocomposites have been employed in photocatalysis,[40,41] sensors,[42–48] solar cells,[49–52] reinforcement,[53–58] thermal conduction,[59–61] lithium ion batteries,[62] adsorbent,[63,64] metamaterials,[65] cryogenic materials,[66] insulator,[67] coating,[68] electromagnetics,[69] phototherapy,[70,71] and electrical conduction,[72,73] functional structural materials,[74,75] and energy storage/conversion materials.[76–80] All these can be studied for future research directions.

Since the fuel cell is still in its immature state, advances in fundamental scientific understanding as well as engineering practices will both boost the development of fuel cell industry. In response to the growing environmental needs, the research on fuel cells is expanding; however, there is plenty of room to propel the technology forward. For example, reducing the overpotentials by looking into the electrode-electrolyte interfaces using advanced probe techniques, such as scanning tunneling electron microscopy, optical reflection

spectroscopy, and synchrotron radiation scattering, which evolve into the in situ probes that can help reveal the details of the charged interface structure; making the ultimate use of surface areas by nanotechnology;[81,82] studying the reaction process itself, involving not only the quantum chemistry that describes any set of reacting atoms, but also the interaction between absorbed species and charge-carrier excitations at the electrolyte-electrode interface. The best prospects for fulfilling the final commercialization are offered by technological improvements based on increased understanding of the fundamentals.

Acknowledgements

This project is supported by the National Natural Science Foundation of China (no. 51673053), Science and Technology Planning Project of Guangdong Province (No.2017A010103039), Natural Science Foundation of Guangdong Province (No.2015A030313506), Applied Basic Research Program (High school Innovation Project 201701D31111183) of Shanxi Province, and Shanxi Province Major Special Project for New Materials.

References

[1] T. R. Cook, D. K. Dogutan, S. Y. Reece, Y. Surendranath, T. S. Teets, D. G. Nocera, *Chem. Rev.* **2010**, *110*, 6474–6502.
[2] C. X. Zhao, X. Wang, W. Zeng, Z. K. Chen, B. S. Ong, K. Wang, L. Deng, G. Xu, *Appl. Phys. Lett.* **2011**, *99*, 053305.
[3] S. S. Chen, C. X. Zhao, A. Y. Mao, R. W. Li, G. Xu, *Synth. Met.* **2014**, *197*, 75–79.
[4] L. Deng, K. Wang, C. X. Zhao, H. Yan, J. F. Britten, G. Xu, *Crystals* **2011**, *1*, 112.
[5] Y. Ma, C. X. Zhao, L. L. Deng, H. Yan, S. S. Chen, G. Xu, *Electrochim. Acta* **2013**, *102*, 127–132.
[6] M. D. Stoller, S. Park, Y. Zhu, J. An, R. S. Ruoff, *Nano Lett.* **2008**, *8*, 3498–3502.
[7] P. Simon, Y. Gogotsi, *Nature Mater.* **2008**, *7*, 845.
[8] G. Lota, K. Fic, E. Frackowiak, *Energy Environ. Sci.* **2011**, *4*, 1592–1605.
[9] B. Seger, P. V. Kamat, *J. Phys. Chem. C* **2009**, *113*, 7990–7995.
[10] E. P. Murray, T. Tsai, S. A. Barnett, *Nature* **1999**, *400*, 649.
[11] Y. Wang J. Clancey, G. Lu, J. Liu, L. Liu, J. Chaudhuri, S. George, M. Xie, S. Wei, Z. Guo, *J. Electrochem. Soc.,* **2016**, *163*, F1–F10.
[12] Y. Wang, Q. He, J. Guo, J H. Wei, H K. Ding, H. Lin, S. Bhana, X. Huang, Z. Luo, T. D. Shen, S. Wei, S Z. Guo, *ChemElectroChem* **2015**, *2*, 559–570.
[13] Y. Wang, Q. He, K. Ding, H. Wei, J. Guo, Q. Wang, R. O'Connor, X. Huang, Z. Luo, T. D. Shen, S. Wei, Z. Guo, *J. Electrochem. Soc.,* **2015**, *162*, F755–F763.
[14] K. Ding, Y. Li, Y. Zhao, L. Liu, H. Gu, L. Liu, L S. Qiu, C. He, J. Liu, Q. Wang, Z. Guo, *Electrochim. Acta* **2014**, *149*, 186–192.
[15] J. Chen, C. X. Zhao, M. M. Zhi, K. Wang, L. Deng, G. Xu, *Electrochim. Acta* **2012**, *66*, 133–138.
[16] C. X. Zhao, K. Wang, H. Yan, G. Xu, *J. Electrochem. Soc.,* **2011**, *158*, B1055–B1059.
[17] H. Rismani-Yazdi, S. M. Carver, A. D. Christy, Z. Yu, K. Bibby, J. Peccia, O. H. Tuovinen, *Bioresour. Technol.* **2013**, *129*, 281–288.
[18] H. W. Kroto, J. R. Heath, S. C> O'Brien, R. F. Curl, R. E. Smalley, *Nature* **1985**, *318*, 162.
[19] W. Krätschmer, L. D. Lamb, K. Fostiropoulos, D. R. Huffman, *Nature* **1990**, *347*, 354.
[20] K. K. Wang, H. Yan, C. X. Zhao, G. Xu, Y. Qi, Y. Wu, N.-X. Hu, *Langmuir* **2010**, *26*, 7686–7689.
[21] H. Yan, C. Zhao, K. Wang, L. Deng, M. Ma, G. Xu, *Appl. Phys. Lett.* **2013**, *102*, 062904.
[22] A. K. Geim, K. S. Novoselov, *Nature Mater.* **2007**, *6*, 183.
[23] P. Sutter, *Nature Mater.* **2009**, *8*, 171.
[24] T.-H. Han, Y. Lee, M.-R. Choi, S.-H. Woo, S.-H. Bae, B. H. Hong, J.-H. Ahn, T.-W. Lee, *Nat. Photonics* **2012**, *6*, 105.
[25] L. L. Deng, C. X. Zhao, Y. Ma, S. S. Chen, G. Xu, *Analytical Methods* **2013**, *5*, 3709–3713.
[26] C. X. Zhao, L. L. Deng, M. Y. Ma, J. R. Kish, G. Xu, *AIP Adv.* **2013**, *3*, 102121.
[27] X. Wang, C. Xinxin Zhao, G. Xu, Z.-K. Chen, F. Zhu, *Sol. Energy Mater. Sol. Cells* **2012**, *104*, 1–6.
[28] C. X. Zhao, L. L. Deng, G. Xu, *Meeting Abstracts* **2013**, MA2013-01, 833.
[29] C. X. Zhao, A. Y. Mao, G. Xu, *Appl. Phys. Lett.* **2014**, *105*, 063302.
[30] C. X. Zhao, K. Wang, J. F. Britten, M. Zhi, M X. Wang, Z. K. Chen, G. Xu, *Thin Solid Films* **2012**, *520*, 5770–5774.
[31] C. X. Zhao, S. Xiao, G. Xu, *J. Appl. Phys.,* **2015**, *118*, 044510.
[32] K. Ding, Y. Wang, H. Yang, C. Zheng, Yanli Cao, H. Wei, Y. Wang, Z. Guo, *Electrochim. Acta* **2013**, *100*, 147–156.
[33] K. Ding, H. Yang, Y. Cao, C. Zheng, S. B. Rapole, Z. Guo, *Mater. Chem. Phys.* **2013**, *142*, 403–411.
[34] K. Ding, Y. Zhao, L. Liu, Y. Cao, Q. Wang, H. Gu, X. Yan, Z. Guo, *Int. J. Hydrogen Energy* **2014**, *39*, 17622–17633.
[35] Y. Wang, Y. Q. He, J. Guo, J. J. Wang, Z. Luo, T. D. Shen, K. Ding, A. Khasanov, S. Wei, Z. Guo, *ACS Appl. Mater. Interfaces* **2015**, *7*, 23920–23931.
[36] Y. Wang, Q. He, H. Wei, J. Guo, J. K. Ding, Q. Wang, Z. Wang, S. Wei, Z. Guo, *Electrochim. Acta* **2015**, *184*, 452–465.
[37] K. Ding, K L. Liu, Y. Cao, X. Yan, H. Wei, Z. Guo, *Int. J. Hydrogen Energy* **2014**, *39*, 7326-7337.
[38] K. Ding, Y. Wang, L. Liu, L. Liu, X. Zhang, J. Z. Guo, *Appl. Electrochem.* **2013**, *43*, 567–574.
[39] K. Ding H. Yang, Y. Cao, C. Zheng, L. Liu, L.L. Liu, Y. Wang, X. Yan, Z. Guo, *Int. J. Electrochem. Sci.* **2013**, *8*, 5343-5358.
[40] B. Song, T. Wang, H. Sun, Q. Shao, J. Zhao, K. Song, L. Hao, L. Wang, Z. Guo, *Dalton Trans.* **2017**, *46*, 15769–15777.
[41] Q. Liu, Q. Jia, J. Zhu, Q. Shao, J. Fan, D. Wang, Y. Yin, *Chin. Chem. Lett.* **2014**, *25*, 752–756.

[42] K. Sun, P. Xie, Z. Wang, T. Su, Q. Shao, J.-E. Ryu, X. Zhang, J. Guo, A. Shankar, J. Li, R. Fan, D. Cao, Z. Guo, *Polymer* **2017**, *125*, 50–57.
[43] Y. Li, B. Zhou, G. Zheng, X. Liu, T. Li, C. Yan, C. Cheng, K. Dai, C. Liu, C. Shen, Z. Guo, *J. Mater. Chem. C* **2018**, *6*, 2258–2269.
[44] H. Liu, W. Huang, X. Yang, K. Dai, G. Zheng, C. Liu, C. Shen, J. Guo, Z. Guo, *J. Mater. Chem. C* **2016**, *4*, 4459–4469.
[45] H. Liu, M. Dong, W. Huang, J. Gao, K. Dai, J. Guo, G. Zheng, C. Liu, C. Shen, Z. Guo, *J. Mater. Chem. C* **2017**, *5*, 73–83.
[46] H. Liu, Y. Li, K. Dai, G. Zheng, C. Liu, C. Shen, X. Yan, J. Guo, Z. Guo, *J. Mater. Chem. C* **2016**, *4*, 157–166.
[47] C. Hu, Z. Li, Y. Wang, J. Gao, K. Dai, G. Zheng, C. Liu, C. Shen, H. Song, Z. Guo, *J. Mater. Chem. C* **2017**, *5*, 2318–2328.
[48] Q. Liu, J. Zhu, T. Sun, H. Zhou, Q. Shao, G. Li, X. Liu, Y. Yin, *RSC Adv.* **2013**, *3*, 2765–2769.
[49] Q. Hou, J. Ren, H. Chen, P. Yang, Q. Shao, M. Zhao, X. Zhao, H. He, N. Wang, Q. Luo, Z. Guo, *ChemElectroChem* **2018**, *5*, 726–731.
[50] Q. Luo, H. Ma, Q. Hou, Y. Li, J. Ren, X. Dai, Z. Yao, Y. Zhou, Y. Xiang, H. Du, H. He, N. Wang, K. Jiang, H. Lin, H. Zhang, Z. Gu, *Adv. Funct. Mater.* **2018**, *28*, 1706777.
[51] W. Hu, T. Liu, X. Yin, H. Liu, X. Zhao, S. Luo, Y. Guo, Z. Yao, J. Wang, N. Wang, H. Lin, Z. Guo, *J. Mater. Chem. A* **2017**, *5*, 1434–1441.
[52] T. Liu, K. Yu, L. Gao, H. Chen, N. Wang, L. Hao, T. Li, H. He, Z. Guo, *J. Mater. Chem. A* **2017**, *5*, 17848–17855.
[53] X. Wang, X. Liu, H. Yuan, H. Liu, C. Liu, T. Li, C. Yan, X. Yan, C. Shen, Guo, *Mater. Des.* **2018**, *139*, 372–379.
[54] C. Wang, M. Zhao, J. Li, J. Yu, S. Sun, S. Ge, X. Guo, F. Xie, B. Jiang, E. K. Wujcik, Y. Huang, N. Wang, Z. Guo, *Polymer* **2017**, *131*, 263–271.
[55] M. Zhao, L. Meng, L. Ma, L. Ma, X. Yang, Y. Huang, J.-E. Ryu, A. Shankar, T. Li, C. Yan, Z. Guo, *Compos. Sci. Technol.* **2018**, *154*, 28–36.
[56] X. Guan, G. Zheng, K. Dai, C. Liu, X. Yan, C. Shen, Z. Guo, *ACS Appl. Mater. Interfaces* **2016**, *8*, 14150–14159.
[57] Z. Hu, Q. Shao, M. G. Moloney, X. Xu, D. Zhang, J. Li, C. Zhang, Y. Huang, *Macromolecules* **2017**, *50*, 1422.
[58] Z. Hu, Q. Shao Q, X. Xu, D. Zhang, Y. Huang, *Comp. Sci Technol.* **2017**, *142*, 294–301.
[59] Y. Guo, G. Xu, X. Yang, K. Ruan, T. Ma, Q. Zhang, J. Gu, Y. Wu, H. Liu, Z. Guo, *J. Mater. Chem. C* **2018**, *6*, 3004–3015.
[60] Y. Song, L. He, X. Zhang, F. Liu, N. Tian, Y. Tang, J. Kong, *J. Phys. Chem. C* **2017**, *121*, 24774–24785.
[61] W. Zhao, J. Kong, H. Liu, Q. Zhuang, J. Gu, Z. Guo, *Nanoscale* **2016**, *8*, 19983–19994.
[62] C. Lin, L. Hu, C. Cheng, K. Sun, X. Guo, Q. Shao, J. Li, N. Wang, Z. Guo, *Electrochim. Acta* **2018**, *260*, 65–72.
[63] J. Huang, Y. Cao, Q. Shao, X. Peng, Z. Guo, *Ind. Eng. Chem. Res.* **2017**, *56*, 10689–10701.
[64] H. Gu, X. Xu, H. Zhang, C. Liang, H. Lou, C. Ma, Y. Li, Z. Guo, J. Gu, *Eng. Sci.* **2018**, in press, doi: 10.30919/espub.es.180308
[65] C. Cheng, R. Fan, Z. Wang, Q. Shao, X. Guo, P. Xie, Y. Yin, Y. Zhang, L. An, Y. Lei, J.-E. Ryu, A. Shankar, Z. Guo, *Carbon* **2017**, *125*, 103–112.
[66] Y. He, S. Yang, H. Liu, Q. Shao, Q. Chen, C. Lu, Y. Jiang, C. Liu, Z. Guo, *J. Colloid Interface Sci.* **2018**, *517*, 40–51.
[67] Z. Wu, S. Gao, L. Chen, D. Jiang, Q. Shao, B. Zhang, Z. Zhai, C. Wang, M. Zhao, Y. Ma, X. Zhang, L. Weng, M. Zhang, Z. Guo, *Macromol. Chem. Phys.* **2017**, *218*, 1700357.
[68] J. Lin, X. Chen, C. Chen, J. Hu, C. Zhou, X. Cai, W. Wang, C. Zheng, P. Zhang, J. Cheng, Z. Guo, H. Liu, *ACS Appl. Mater. Interfaces* **2018**, *10*, 6124–6136.
[69] K. Zhang, G.-H. Li, L.-M. Feng, N. Wang, J. Guo, K. Sun, K.-X. Yu, J.-B. Zeng, T. Li, Z. Guo, M. Wang, *J. Mater. Chem. C* **2017**, *5*, 9359–9369.
[70] Z. Hu, C. Wang, F. Zhao, X. Xu, S. Wang, L. Yu, D. Zhang, Y. Huang, *Nanoscale* **2017**, *9*, 8825–8833.
[71] Z. Hu, D. Zhang, L. Yu, Y. Huang, *J. Mater. Chem. B* **2018**, *6*, 518–526.
[72] J. Huang, C. Mao, Y. Zhu, W. Jiang, X. Yang, *Carbon* **2014**, *73*, 267–274.
[73] C. Mao, Y. Zhu, W. Jiang, *ACS Appl. Mater. Interfaces* **2012**, *4*, 5281–5286.
[74] G. Yu, L. Yang, J. Guo, M. Patel, A. Bafana, X. Wang, B. Qiu, C. Jeffryes, S. Wei, Z. Guo, E. Wujcik, *Adv. Compos. Hybrid Mater.* **2018**, *1*, 56–78.
[75] Z. Hu, Q. Shao, Y. Huang, L. Yu, D. Zhang, X. Xu, J. Lin, H. Liu, Z. Guo, *Nanotechnology* **2018**, *29*, 185602.
[76] W. Deng, T. Kang, H. Liu, J. Zhang, N. Wang, N. Lu, Y. Ma, A. Umar, Z. Guo, *Sci. Adv. Mater.* **2018**, in press, doi: 10.1166/sam.2018.3279.
[77] H. Wei, H. Gu, J. Guo, X. Yan, J. Liu, D. Cao, X. Wang, S. Wei, Z. Guo, *Adv. Compos. Hybrid Mater.* **2018**, *1*, 127–134.
[78] Y. Guo, Y. Li, X. Lou, J. Guan, Y. Li, X. Mai, H. Liu, C. X. Zhao, N. Wang, C. Yan, G. Gao, H. Yuan, J. Dai, Z. Guo, *J. Mater. Sci.* **2018**, in press, doi: 10.1007/s10853-018-2229-0.
[79] F. Fan, X. Yang, L. Shao, *Adv. Compos. Hybrid Mater.* **2018**, *1*, 32–55.
[80] Q. Luo, H. Ma, F. Hao, Q. Hou, J. Ren, L. Wu, Z. Yao, Y. Zhou, N. Wang, K. Jiang, H. Lin, Z. Guo, *Adv. Funct. Mater.* **2017**, *27*, 1703068.
[81] J. Zhao, S. Ge, L. Liu, Q. Shao, X. Mai, C. X. Zhao, L. Hao, T. Wu, Z. Yu, Z. Guo, *Indus. Eng. Chem. Res.* **2018**, *57*, 231–241.
[82] C. Wang, B. Mo, Z. He, Q. Shao, D. Pan, E. Wujick, J. Guo, X. Xie, X. Xie, Z. Guo, *J. Membr. Sci.* **2018**, 556, 118–125.

Received: January 30, 2018
Accepted: March 22, 2018
Published online on April 19, 2018

